Vlaams Instituut voor de Zee
Flanders Marine Institute

ELSEVIER

Journal of Marine Systems 8 (1996) 107–117

JOURNAL OF MARINE SYSTEMS

On the numerical treatment of a lateral boundary layer in a shallow sea model

E. Deleersnijder [1]

Institut d'Astronomie et de Géophysique G. Lemaître (Unité ASTR), Université Catholique de Louvain, 2 Chemin du Cyclotron, B-1348 Louvain-la-Neuve, Belgium

Received 20 August 1994; accepted 7 March 1995

Abstract

We consider the flow in an idealized, shallow sea, steady state, coastal boundary layer. The driving force is the along-shore slope of the sea surface. The latter is balanced by bottom stress and horizontal diffusion of momentum. The momentum equation governing the along-shore velocity is derived. Suitable assumptions are made in order to obtain a closed form solution. The governing equation is then discretized on the B- and C-grid, with slip (together with an appropriate wall function) and no-slip boundary conditions. The discrete solutions are compared with the exact one, according to different standards: the errors affecting pointwise values, as well as fluxes, are evaluated. The errors are estimated as a function of the ratio of the boundary layer width to the grid size, which ranges from 0.01 (non resolved boundary layer) to 100 (well resolved boundary layer). In general, the errors are small. However, for the B-grid with a no-slip boundary condition, the flux crossing the grid box adjacent to the coast is in error by a factor of $\approx 1/2$ when the width of the boundary layer is much smaller than the grid size. The C-grid, when implemented with a slip condition, permits the highest overall accuracy.

1. Introduction

To illustrate that too simple models may lead to irrelevant results, Nihoul (1994) — hereafter referred to as Nihoul — examined a classical boundary layer problem (Eqs. 5–9 in Nihoul). The equation considered contained a small parameter, α, appearing as a factor of the highest order derivative. Setting this parameter to zero abruptly changed the order of magnitude of the solution by a factor α^{-1}. Therefore, disregarding terms that are thought to be small everywhere, except in narrow boundary layers, may be detrimental to the accuracy of the solution in the whole domain of interest.

Nihoul's example, though striking, may not be relevant to the models presently used in oceanography — and it may be somewhat surprising that neither Davies (1994) nor Salomon (1994) picked out this point. For example, it is doubtful that any such singular perturbation problem is spoiling the results of the now standard primitive equation model POM (Princeton Ocean Model), originally described by Blumberg and Mellor (1987), or MOM (GFDL's Modular Ocean Model), first devised by Bryan (1969). This probably holds true

[1] Tel: 32-10-47.26.76 or 32-10-47.32.97, Fax: 32-10-47.47.22, e-mail: ericd@astr.ucl.ac.be. Research Associate, National Fund for Scientific Research of Belgium.

SSDI 0924-7963(95)00043-7

for all of the models based on similar equations and numerical techniques. In models resting on important simplifying assumptions, such as quasi-geostrophic models, the boundary conditions have been carefully designed in order to avoid singular perturbation problems.

We are thus convinced that errors of the magnitude evoked by Nihoul no longer exist in currently used models. However, less important, and perhaps more subtle, questions associated with boundary layers may still deserve some attention.

For example, one has hardly ever examined the accuracy of the numerical treatment of the coastal boundary layer, as well as its influence on the flow outside this boundary layer. This is the reason that we have decided to devote some attention to this problem.

In this paper, we are going to study different ways of treating, in a numerical model, the boundary layer adjacent to the coastline. We have no intention of drawing conclusions that may be valid for every type of flow. Instead, we will concentrate on a particular shallow water case, i.e., the general circulation in the region of the Bering Strait. An idealized model thereof will be considered and somewhat surprising results will be obtained.

2. The boundary layer problem

In the domain of interest, the general circulation — defined as the flow averaged over a period of time such that tidal motions are filtered out — is mainly driven by the surface of the Pacific being higher than that of the Arctic (Coachman and Aagaard, 1966; Stigebrandt, 1984). For the present discussion, this northward flow may be considered as steady and the role of the wind stress may be neglected (Deleersnijder, 1994). The depth-averaged models that have been applied to this region achieved appreciable realism (Overland and Roach, 1987; Spaulding et al., 1987; Brasseur, 1991). We thus consider two-dimensional, time-independent governing equations, with no wind forcing. Since the sea surface elevation is much smaller than the height of the water column (Overland and Roach, 1987; Spaulding et al., 1987), the sea depth is considered to be equal to its reference, unperturbed value. Assuming a rectilinear coastline, the continuity and momentum equations read

$$\frac{\partial(hu)}{\partial x}+\frac{\partial(hv)}{\partial y}=0, \tag{1}$$

$$u\frac{\partial u}{\partial x}+v\frac{\partial u}{\partial y}-fv=-g\frac{\partial \eta}{\partial x}+A\left(\frac{\partial^2 u}{\partial x^2}+\frac{\partial^2 u}{\partial y^2}\right)-\frac{\tau^x}{h}, \tag{2}$$

$$u\frac{\partial v}{\partial x}+v\frac{\partial v}{\partial y}+fu=-g\frac{\partial \eta}{\partial y}+A\left(\frac{\partial^2 v}{\partial x^2}+\frac{\partial^2 v}{\partial y^2}\right)-\frac{\tau^y}{h}, \tag{3}$$

where x and y are the along- and cross-shore coordinates (Fig. 1); u and v represent the velocity components associated with the x and y axes; η is the sea surface elevation — positive upwards; h, f, g and A denote the unperturbed depth of the sea, the Coriolis factor, the gravitational acceleration and the horizontal viscosity — assumed constant, respectively; the bottom stress components are τ^x and τ^y.

In the vicinity of the coast, it may be hypothesized that the variations of the velocity in the

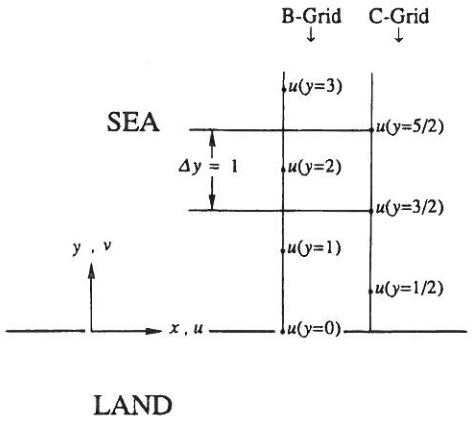

Fig. 1. Illustration of the B- and C-grid discretizations of the along-shore velocity, u, in the coastal boundary layer. Here, dimensionless variables are used.

along-shore direction are negligible relative to the variations in the cross-shore direction. Eq. (1) may thus be reduced to $\partial(h\nu)/\partial y = 0$, which, together with the impermeability condition of the coast, implies that ν must be zero everywhere. Assuming that τ^y is zero when ν is zero, Eqs. (2)–(3) transform to semi-geostrophic equations of motion

$$0 = -g\frac{\mathrm{d}\eta}{\mathrm{d}x} + A\frac{\mathrm{d}^2u}{\mathrm{d}y^2} - \frac{\tau^x}{h}, \tag{4}$$

$$fu = -g\frac{\mathrm{d}\eta}{\mathrm{d}y}. \tag{5}$$

To account for the effect of the tides on the long term circulation, Overland and Roach (1987) suggest parameterizing the bottom stress as

$$\frac{\tau^x}{h} = Ku \tag{6}$$

with

$$K = \frac{C_D}{h}(|u| + u_T), \tag{7}$$

where C_D is an approriate drag coefficient and u_T (≥ 0) denotes a velocity scale which is a function of the tidal amplitude. Setting $u_T = 0$, we recover the most classical parameterization (e.g., Nihoul, 1980). As the coast is approached, both $|u| + u_T$ and h tend to zero. It is tempting to assume that $|u| + u_T$ and h behave in such a way that K is constant, leading to a linear parameterization of τ^x/h.

The along-shore slope of the sea surface is the driving force of the flow. For simplicity, the latter is defined to be constant, $F = -g\ \partial\eta/\partial x$. This expression of the forcing is obviously in agreement with the flow being forced by the sea surface slope.

According to the discussion above, the sole equation we have to study is

$$A\frac{\mathrm{d}^2u}{\mathrm{d}y^2} - Ku = -F, \tag{8}$$

Sufficiently far away from the coastline, located at $y = 0$, it may be imagined that the variations of u are sufficiently small that the bottom stress and the driving force approximately balance each other. This would be in agreement with model results of Deleersnijder (1994). Close to the shore, however, this balance of forces can no longer prevail since Ku must tend to zero. It is there that horizontal diffusion of momentum should become significant.

It is not clear what parameterization of the horizontal diffusion of momentum is best suited to the present problem. In fact, many expressions have been suggested (see, for instance, Nihoul, 1975; Mellor and Blumberg, 1985; Deleersnijder and Wolanski, 1990). Here, we adopted the form leading to the simplest analytical solution.

Several crude approximations have been made. Although physical considerations were not absent, the need to obtain closed form solutions has been the prevailing criterion for elaborating the present model. This is typical of the radiognostic approach — according to Nihoul's classification of models.

3. Analytical and numerical solutions

It is useful to introduce the following dimensionless variables

$$(y', u') = \left(\frac{y}{L}, \frac{Ku}{F}\right), \tag{9}$$

where L is an appropriate length scale. As we are interested in numerical solutions, it is convenient to set $L = \Delta y$, where Δy is the grid spacing in the cross-shore direction — which is supposed constant, for simplicity. Introducing the variables defined above into Eq. (8), dropping the primes, the following dimensionless momentum equation is obtained

$$\epsilon^2\frac{\mathrm{d}^2u}{\mathrm{d}y^2} - u = -1, \tag{10}$$

with

$$\epsilon^2 = \frac{A}{\Delta y^2 K}. \tag{11}$$

According to the discussion above, the boundary conditions for Eq. (10) are $u(y=0)=0$ and $u(y\to\infty)=1$, leading to

$$u(y)=1-\exp(-y/\epsilon). \tag{12}$$

Thus, ϵ may be seen as the dimensionless thickness of the coastal boundary layer, which is to be compared with the dimensionless grid size $\Delta y=1$. If ϵ is much larger than unity, then the boundary layer is well resolved by the numerical grid; otherwise, the boundary layer is, at best, poorly resolved.

To design a conservative discretization of Eq. (10), it is worth recalling that $\epsilon^2\,\mathrm{d}^2u/\mathrm{d}y^2$ may be re-written as $\mathrm{d}\sigma/\mathrm{d}y$, where σ is the stress associated with the horizontal diffusion of momentum. Of course, σ is given by $\sigma=\epsilon^2\,\mathrm{d}u/\mathrm{d}y$. It follows that Eq. (10) may be discretized as

$$\bar{\sigma}(y+1/2)-\bar{\sigma}(y-1/2)-\bar{u}(y)=-1, \tag{13}$$

with

$$[\bar{\sigma}(y+1/2),\bar{\sigma}(y-1/2)] = \epsilon^2[\bar{u}(y+1)-\bar{u}(y),\bar{u}(y)-\bar{u}(y-1)], \tag{14}$$

where the overbar refers to the value of the corresponding variable obtained from the numerical scheme. The along-shore velocity verifying Eqs. (13) and (14) is of the form (Bender and Orszag, 1978)

$$\bar{u}(y)=1-\bar{U}\exp(-y/\bar{\epsilon}), \tag{15}$$

where $\bar{U}$ is a constant to be determined from the coastal boundary condition. The thickness of the numerical boundary layer is $\bar{\epsilon}=-(\ln r)^{-1}$, with

$$r=\frac{1+2\epsilon^2-(1+4\epsilon^2)^{1/2}}{2\epsilon^2}. \tag{16}$$

It is easily seen that $0<r<1$, so that $\bar{\epsilon}>0$.

In many calculations carried out below, use is made of the relation $(1-r)^2\epsilon^2=r$, which may be derived from Eq. (16) after elementary manipulations.

If the boundary layer is well resolved, i.e., if $\epsilon\to\infty$, then $\bar{\epsilon}$ is asymptotic to ϵ, as expected. We indeed have

$$\bar{\epsilon}\sim\epsilon+\frac{1}{24\epsilon},\quad \epsilon\to\infty. \tag{17}$$

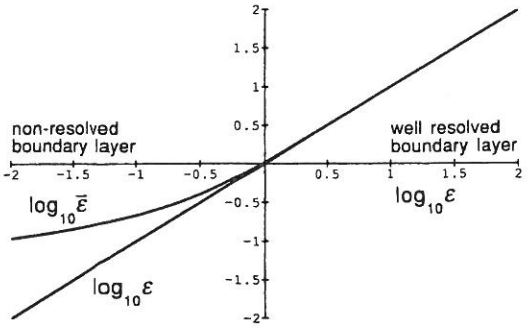

Fig. 2. Thickness of the numerical boundary layer, $\bar{\epsilon}$, as a function of the exact thickness, ϵ. Dimensionless widths are considered.

As ϵ tends to zero, the difference $\bar{\epsilon}-\epsilon$ becomes relatively larger, as illustrated in Fig. 2. In any case, the thickness of the numerical boundary layer, $\bar{\epsilon}$, is larger than its exact counterpart, ϵ (Fig. 2).

The asymptotic expansions presented in this article have been derived with the help of Mathematica™ (Wolfram, 1988), by means of the built-in object "Series".

Two grid point arrangements may be considered. First, it may be assumed that a velocity node is located on the coastline, as is usually the case when the B-grid is used (e.g., Bryan, 1969). Hence, the wet grid points are at $y=1, 2, 3,\ldots$ (Fig. 1). With the C-grid, the along-shore velocity is generally discretized at $y=1/2, 3/2, 5/2,\ldots$ (Fig. 1).

Two types of numerical boundary condition may be implemented in the coastal region. A no-slip condition may be prescribed by setting $\bar{u}(0)=0$ with the B-grid, and $\bar{u}(-1/2)+\bar{u}(1/2)=0$ if the C-grid is selected. When a slip boundary condition is preferred, the lateral stress $\bar{\sigma}$ must be prescribed at $y=1/2$ and $y=0$ for the B- and C-grid, respectively. To do so, the exact expression of the lateral stress,

$$\sigma(y)=\epsilon\exp(-y/\epsilon), \tag{18}$$

is used. The latter formula is sometimes called "the wall function". In other words, we impose

$$\bar{\sigma}(1/2)=\sigma(1/2)=\epsilon\exp[-1/(2\epsilon)], \tag{19}$$

Table 1
Features of the discrete along-shore velocity, according to the numerical lattice (B- or C-grid) and the coastal boundary condition (slip or no-slip)

	B-grid and no-slip	B-grid and slip	C-grid and no-slip	C-grid and slip
Wet grid points:	$y = 1, 2, 3, \ldots$ ($y_c = 1$)	$y = 1, 2, 3, \ldots$ ($y_c = 1$)	$y = 1/2, 3/2, 5/2, \ldots$ ($y_c = 1/2$)	$y = 1/2, 3/2, 5/2, \ldots$ ($y_c = 1/2$)
Boundary condition:	$\bar{u}(0) = 0$	$\bar{\sigma}(1/2) = \epsilon\, e^{-1/(2\epsilon)}$	$\bar{u}(-1/2) + \bar{u}(1/2) = 0$	$\bar{\sigma}(0) = \epsilon$
Value of $\bar{U}$:	1	$r^{-1/2}\, e^{-1/(2\epsilon)}$	$2\, r^{1/2}\, (1+r)^{-1}$	1

for the B-grid, and

$$\bar{\sigma}(0) = \sigma(0) = \epsilon, \tag{20}$$

for the C-grid.

Having defined two types of numerical lattices, as well as two types of boundary conditions, four discrete solutions may be obtained, which are all of the form (15). All important features of these solutions are collected in Table 1.

It is now necessary to compare these solutions with the exact one.

4. Assessment of the discrete solutions

Various ways of evaluating the "distance" of the numerical solutions to the exact one will be considered. Both pointwise and integral error measures will be evaluated.

4.1. Pointwise values

We first concentrate on a pointwise error measure. To do so, it is convenient to introduce the variable

$$\Delta u = u - \bar{u}. \tag{21}$$

We may first examine the value of Δu at $y = y_c$, i.e., at the wet grid point nearest to the coastline (Table 2). In general, it is there that $|\Delta u|$ is maximum.

For the B-grid, $\Delta u(y_c)$ does not exceed 0.05, which means that the discrete solution is quite close to the exact one, no matter the value of ϵ (Fig. 3). It is when ϵ is of order 1 that $\Delta u(y_c)$ is maximum. At first, this might seem somewhat surprising, but an explanation thereof is easily found. For large values of ϵ, the boundary layer is well resolved by the numerical grid, so that it is

Table 2
Pointwise error measure Δu evaluated at the wet node nearest to the coastline. The integral $|\Delta u|_{RSS}$ is also evaluated. For both error measures, the exact values, together with asymptotic expansions for $\epsilon \ll 1$ (non resolved boundary layer) and $\epsilon \gg 1$ (well resolved boundary layer) are given

	B-grid and no-slip	B-grid and slip	C-grid and no-slip	C-grid and slip
error $\Delta u(y_c)$:	$r\text{-}e^{-1/\epsilon}$	$r^{1/2}\, e^{-1/(2\epsilon)}\text{-}e^{-1/\epsilon}$	$2\, r(1+r)^{-1}\text{-}e^{-1/(2\epsilon)}$	$r^{1/2}\text{-}e^{-1/(2\epsilon)}$
$\epsilon \to 0$	$\sim \epsilon^2\text{-}2\epsilon^4$	$\sim (\epsilon\text{-}\epsilon^3)e^{-1/(2\epsilon)}$	$\sim 2\epsilon^2\text{-}6\epsilon^4$	$\sim \epsilon\text{-}\epsilon^3$
$\epsilon \to \infty$	$\sim 1/(24\epsilon^3)\text{-}1/(24\epsilon^4)$	$\sim 1/(48\epsilon^3)\text{-}1/(48\epsilon^4)$	$\sim -1/(8\epsilon^2) + 1/(12\epsilon^3)$	$\sim 1/(48\epsilon^3)\text{-}1/(96\epsilon^4)$
Error $\lvert\Delta u\rvert_{RSS}$:	$[r^2(1\text{-}r^2)^{-1}\text{-}2r(e^{1/\epsilon}\text{-}r)^{-1} + (e^{2/\epsilon}\text{-}1)^{-1}]^{1/2}$	$[re^{-1/\epsilon}(1\text{-}r^2)^{-1}\text{-}2r^{1/2}(e^{3/(2\epsilon)}\text{-}re^{1/(2\epsilon)})^{-1} + (e^{2/\epsilon}\text{-}1)^{-1}]^{1/2}$	$[4r^2(1+r)^{-3}(1\text{-}r)^{-1}\text{-}4r(1+r)^{-1}e^{1/(2\epsilon)}(e^{1/\epsilon}\text{-}r)^{-1} + e^{1/\epsilon}(e^{2/\epsilon}\text{-}1)^{-1}]^{1/2}$	$[r(1\text{-}r^2)^{-1}\text{-}2r^{1/2}e^{1/(2\epsilon)}(e^{1/\epsilon}\text{-}r)^{-1} + e^{1/\epsilon}(e^{2/\epsilon}\text{-}1)^{-1}]^{1/2}$
$\epsilon \to 0$	$\sim \epsilon^2\text{-}2\epsilon^4$	$\sim (\epsilon\text{-}\epsilon^3)\, e^{-1/(2\epsilon)}$	$\sim 2\epsilon^2\text{-}6\epsilon^4$	$\sim \epsilon\text{-}\epsilon^3$
$\epsilon \to \infty$	$\sim 1/(48\epsilon^{3/2})$ $\text{-}13/(7680\epsilon^{7/2})$	$\sim 1/(48\epsilon^{3/2})$ $\text{-}1/(96\epsilon^{5/2})$	$\sim \sqrt{13}/(48\epsilon^{3/2})\text{-}$ $233\sqrt{13}/(33280\epsilon^{7/2})$	$\sim 1/(48\epsilon^{3/2})\text{-}13/(7680\epsilon^{7/2})$

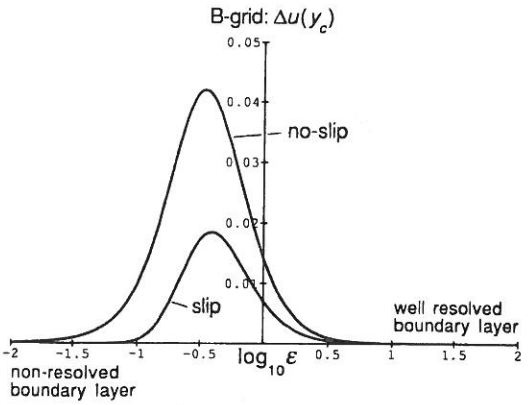

Fig. 3. Error in the discrete along-shore velocity, $\Delta u = u - \bar{u}$, on the B-grid at the wet node nearest to the coastline, which is located at $y_c = 1$. The solutions corresponding to slip and no-slip numerical boundary conditions are considered. The errors are represented as a function of the exact, dimensionless boundary layer width, ϵ.

natural that the error affecting the numerical solution is small. On the other hand, when ϵ is small, the grid spacing is much larger than the width of the boundary layer, so that the first wet grid point is well outside the boundary layer. In this case, the bottom stress is approximately balanced by the forcing, so that $\bar{u}$ must be very close to u. This is confirmed by the asymptotic expansions presented in Table 2, which, together with Fig. 3, show that the slip boundary condition leads to much better results than the no-slip. In other words, although the B-grid is naturally suited to a no-slip condition, it is the slip condition that performs better.

For the C-grid, the behaviour of $\Delta u(y)$ as a function of ϵ is more complex (Fig. 4 and Table 2). As for the B-grid, the error tends to zero as ϵ or ϵ^{-1} approaches zero. If the boundary layer is well resolved, the slip boundary condition should be preferred. But, in the opposite situation, for $\epsilon \to 0$, it is the no-slip condition that permits the highest accuracy. In Fig. 4, for completeness, we have also displayed Δu for a simplistic, and inconsistent, no-slip condition consisting of imposing $u(-1/2) = 0$. The discrete solution corresponding to the latter boundary condition is worse than the others, except for $\epsilon \lesssim 0.1$. Hence, when the boundary layer is much narrower than a grid box, it is desirable to resort to a non-consistent, and seemingly irrelevant, boundary condition! However, the gain in accuracy achieved in this case is so small and the magnitude of the error occuring in the region $\epsilon \gtrsim 0.1$ is so large — relative to errors affecting the other solutions — that this option is probably not acceptable. We will thus not further investigate its properties.

Overall, $|\Delta u(y_c)|$ is larger for the C-grid. This does however not imply that the B-grid enables a better treatment of the coastal boundary layer. We must bear in mind that y_c has different values for the two types of grid, implying that it is not fair to compare Fig. 3 and Fig. 4. In fact, there is probably no indisputable way of comparing the B- and C-grid numerical solutions as regards the treatment of the coastal boundary layer. It is nevertheless tempting to use expression (15) as if every value of y were permitted, which would allow evaluating Δu at the same point for the two grids, at $y = 1$ say. Doing so we obtain Fig. 5, showing that $\Delta u(y = 1)$ has the same order of magnitude for the B- and C-grids. According to this somewhat artificial standard, the B-grid with a slip condition generally performs better than the other types of discretization.

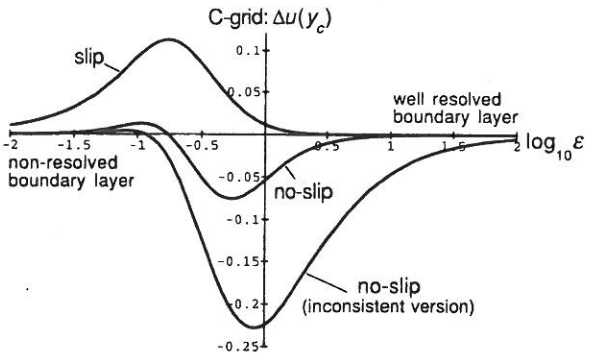

Fig. 4. Error in the discrete along-shore velocity, $\Delta u = u - \bar{u}$, on the C-grid at the wet node nearest to the coastline, which is located at $y_c = 1/2$. The solutions corresponding to slip and no-slip numerical boundary conditions are considered. The error affecting the inconsistent no-slip solution — in which $\bar{u}(-1/2) = 0$ – is also displayed. The errors are represented as a function of the exact, dimensionless boundary layer width, ϵ.

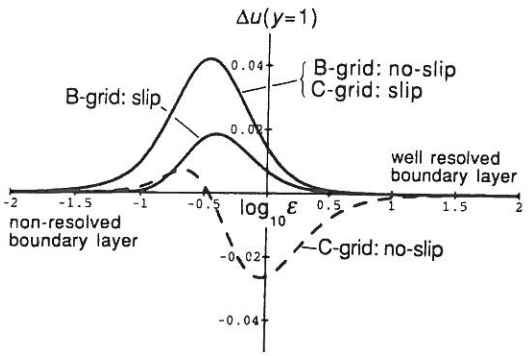

Fig. 5. Error in the discrete along-shore velocity, $\Delta u = u - \bar{u}$, on the B- and C-grid, evaluated at $y = 1$, which is a somewhat artificial measure for the C-grid. The solutions corresponding to slip and no-slip numerical boundary conditions are considered. The errors are represented as a function of the exact, dimensionless boundary layer width, ϵ.

So far we have concentrated on a local measure of the difference between u and $\bar{u}$, i.e., $\Delta u(y_c)$. A more global expression should also be evaluated. For instance, we may calculate the root of the sum of the squares of Δu taken over all wet nodes:

$$|\Delta u|_{\mathrm{RSS}} = \left\{ \sum_{y=y_c}^{\infty} [\Delta u(y)]^2 \right\}^{1/2}. \tag{22}$$

Because $|\Delta u|$ is in general maximum at $y = y_c$, the conclusions that can be drawn from the study of $\Delta u(y_c)$ are qualitatively in agreement with those ensuing from the expression above, as is confirmed by Fig. 6 and Table 2. In particular, the asymptotic expansion of $|\Delta u|_{\mathrm{RSS}}$ as $\epsilon \to 0$ is equivalent to that of $\Delta u(y_c)$ (Table 2), because

$$\lim_{\epsilon \to 0} \frac{\epsilon^{-a}\left\{ [|\Delta u|_{\mathrm{RSS}}]^2 - [\Delta u(y_c)]^2 \right\}}{[\Delta u(y_c)]^2}$$

$$= \lim_{\epsilon \to 0} \frac{\epsilon^{-a} \sum_{y=y_c+1}^{\infty} [\Delta u(y)]^2}{[\Delta u(y_c)]^2} = 0, \tag{23}$$

where a is a positive constant. Further analysis of $|\Delta u|_{\mathrm{RSS}}$ is obviously not necessary.

4.2. Fluxes

The pointwise values of the velocity are also used for evaluating advective fluxes in every — conservative — numerical procedure. In this case, a pointwise value is regarded as an approximation to the average of the velocity along the relevant grid box interface.

The present analysis is restricted to the constant-depth case. Accordingly, we examine integrals of the form

$$\phi(y_1, y_2) = \int_{y_1}^{y_2} u \, \mathrm{d}y, \tag{24}$$

which may be regarded as the along-shore water "flux" crossing the segment $[y_1, y_2]$.

The flux crossing the grid box adjacent to the coast is defined as $\phi(0, 1) = 1 - \epsilon + \epsilon \exp(-1/\epsilon)$. The numerical counterpart of $\phi(0, 1)$ is

$$\bar{\phi}(0, 1) = \frac{\bar{u}(0) + \bar{u}(1)}{2}, \tag{25}$$

for the B-grid, and

$$\bar{\phi}(0,1) = \bar{u}(1/2), \tag{26}$$

for the C-grid.

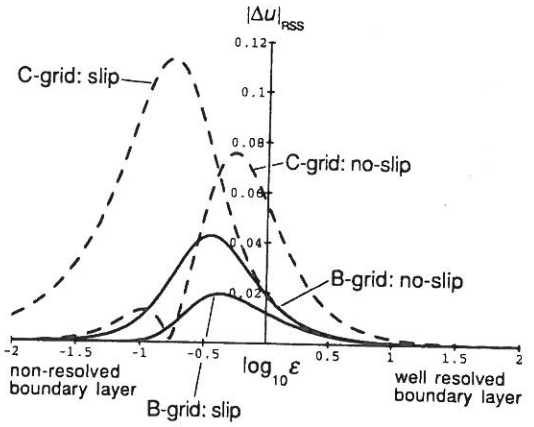

Fig. 6. Global measure of the error, $|\Delta u|_{\mathrm{RSS}}$, affecting the along-shore velcity. The B- and C-grid solutions are considered, according to slip and no-slip conditions in the coastal boundary layer. The errors are represented as a function of the exact boundary layer width, ϵ.

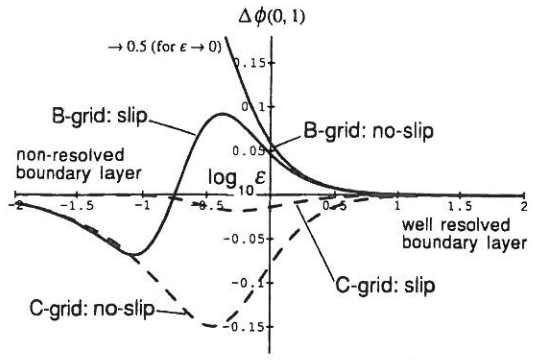

Fig. 7. Error in the water flux crossing the grid box adjacent to the coast, $\Delta\phi(0, 1) = \phi(0, 1) - \bar{\phi}(0, 1)$, on the B- and C-grids. The solutions corresponding to slip and no-slip numerical boundary conditions are considered. The errors are represented as a function of the exact, dimensionless boundary layer width, ϵ.

As may be seen in Fig. 7 and Table 3, the difference $\Delta\phi(0, 1) = \phi(0, 1) - \bar{\phi}(0, 1)$ is smallest for the C-grid with a slip boundary condition. With the noticeable exception of the B-grid with a no-slip boundary condition, $|\Delta\phi(0, 1)|$ is maximum for $0.1 \lesssim \epsilon \lesssim 1$ and very small if the boundary layer is well resolved ($\epsilon \gg 1$) or not resolved at all ($\epsilon \ll 1$). This may be explained by invoking arguments similar to those used to understand the behaviour of the pointwise error measure $\Delta u(y_c)$.

When $\epsilon \ll 1$, the along-shore velocity is close to 1 everywhere, except in a narrow boundary layer adjacent to the coast. Hence, $\phi(0, 1)$ is close to 1. For the B-grid with a no-slip boundary condition, however, $\bar{\phi}(0, 1)$ does not tend to 1, because $\bar{u}(0)$ is precribed to be zero while $\bar{u}(1) \approx 1$, so that $\bar{\phi}(0, 1) \approx 1/2$.

This drawback of the B-grid may be circumvented by implementing a slip boundary condition, as clearly shown in Table 3 and Fig. 7. This is readily achieved in an idealized case — such as that treated herein — where the relevant asymptotic expressions are easily derived. In a more realistic case, however, the no-slip boundary condition is appealing, because it does not require a prior asymptotic study of the coastal boundary layer dynamics — which is likely to be quite intricate and plagued by large uncertainties. When $\epsilon \ll 1$, an alternative, simplified slip boundary condition for the B-grid might be implemented, i.e., $\bar{u}(0) = \bar{u}(1)$. In the present idealized case, this would lead to $\bar{u}(y) = 1$, $\Delta u(1) \sim -\exp(-1/\epsilon)$ and $\Delta\phi(0, 1) \sim -\epsilon$ for $\epsilon \to 0$. This behaviour is much more desirable than that obtained with the no-slip condition. A detailed study of this modified boundary condition should be conducted, including numerical experiments with a realistic model.

A more global error measure is also of interest, for instance $\Delta\phi(0, \infty) = \phi(0, \infty) - \bar{\phi}(0, \infty)$. The flux $\bar{\phi}(0, \infty)$ is computed as

$$\bar{\phi}(0,\infty) = \frac{\bar{u}(0)}{2} + \sum_{y=1}^{\infty} \bar{u}(y), \tag{27}$$

$$\bar{\phi}(0,\infty) = \sum_{y=1/2}^{\infty} \bar{u}(y), \tag{28}$$

for the B- and C-grid, respectively. Not surprisingly, the behaviour of $\Delta\phi(0, \infty)$ is quite similar to that of $\Delta\phi(0, 1)$ (Fig. 8 and Table 3).

Table 3
Error in the along-shore flux crossing the grid box adjacent to the coast, $\Delta\phi(0, 1)$. The integral of the flux error over the computational domain, $\Delta\phi(0, \infty)$, is also evaluated. For both error measures, the exact values, together with asymptotic expansions for $\epsilon \ll 1$ (non resolved boundary layer) and $\epsilon \gg 1$ (well resolved boundary layer) are given

	B-grid and no-slip	B-grid and slip	C-grid and no-slip	C-grid and slip
Error $\Delta\phi(0, 1)$:	$1/2 + r/2 + \epsilon\, e^{-1/\epsilon} - \epsilon$	$r^{-1/2}(1 + r)\, e^{-1/(2\epsilon)}/2 + \epsilon\, e^{-1/\epsilon} - \epsilon$	$2\, r(1 + r)^{-1} + \epsilon\, e^{-1/\epsilon} - \epsilon$	$r^{1/2} + \epsilon\, e^{-1/\epsilon} - \epsilon$
$\epsilon \to 0$	$\sim 1/2 - \epsilon$	$\sim -\epsilon + e^{-1/(2\epsilon)}/(2\epsilon)$	$\sim -\epsilon + 2\epsilon^2$	$\sim -\epsilon^3 + 2\epsilon^5$
$\epsilon \to \infty$	$\sim 1/(12\epsilon^2) - 1/(48\epsilon^3)$	$\sim 1/(12\epsilon^2) - 1/(24\epsilon^3)$	$\sim -1/(6\epsilon^2) + 5/(48\epsilon^3)$	$\sim -1/(24\epsilon^2) + 1/(24\epsilon^3)$
Error $\Delta\phi(0, \infty)$:	$(1 + r)(1 - r)^{-1}/2 - \epsilon$	$r^{-1/2}(1 + r)(1 - r)^{-1}\, e^{-1/(2\epsilon)}/2 - \epsilon$	$2\, r(1 - r^2)^{-1} - \epsilon$	0
$\epsilon \to 0$	$\sim 1/2 - \epsilon$	$\sim -\epsilon + e^{-1/(2\epsilon)}/(2\epsilon)$	$\sim -\epsilon + 2\epsilon^2$	0
$\epsilon \to \infty$	$\sim 1/(8\epsilon) - 1/(128\epsilon^3)$	$\sim 1/(8\epsilon) - 1/(48\epsilon^2)$	$\sim -1/(8\epsilon) - 3/(128\epsilon^3)$	0

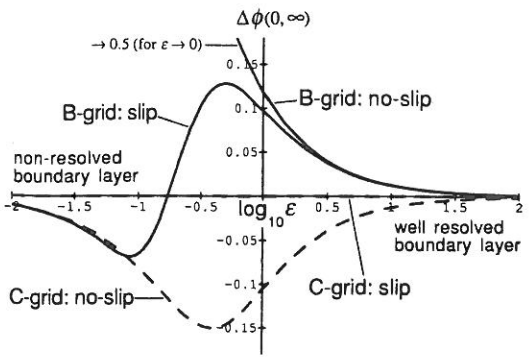

Fig. 8. Error in the water flux crossing the whole computational domain, $\Delta\phi(0, \infty) = \phi(0, \infty) - \bar{\phi}(0, \infty)$, on the B- and C-grids. The solutions corresponding to slip and no-slip numerical boundary conditions are considered. The errors are represented as a function of the exact, dimensionless boundary layer width, ϵ.

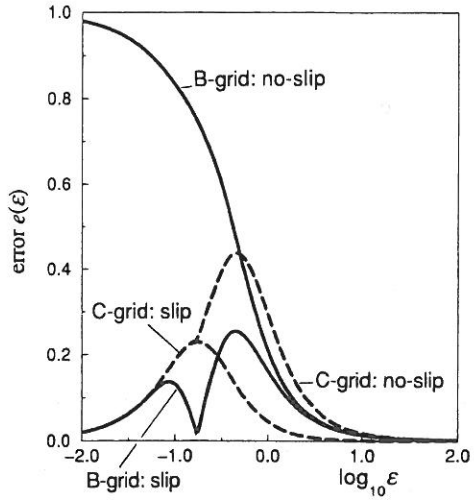

Fig. 9. Overall error measure $e(\epsilon)$ — as defined in Eq. (31). The B- and C-grids, with slip and no-slip boundary conditions, are considered. The large error associated with the no-slip B-grid solution is mainly due to the water flux crossing the grid box adjacent to the coast being ill represented.

It must be stressed that $\Delta\phi(0, \infty)$ is zero for every value of ϵ when the C-grid with a slip condition is considered. This favourable property ensues from the conservative nature of the algorithm. Combining Eqs. (10) and (24), we have

$$\phi(0,\infty) = \int_0^\infty \mathrm{d}y - \sigma(0), \tag{29}$$

while Eqs. (13), (14) and (28) lead to

$$\bar{\phi}(0,\infty) = \sum_{y=1/2}^{\infty} 1 - \bar{\sigma}(0). \tag{30}$$

By virtue of Eq. (20), $\sigma(0) = \bar{\sigma}(0)$, so that $\phi(0, \infty) = \bar{\phi}(0, \infty)$. Hence, $\Delta\phi(0, \infty)$ is identically zero.

4.3. Overall error measure

In the preceding section, a detailed analysis of four types of error measure has been performed. It may also be found desirable to derive a more global — and simple — estimate of the accuracy of the numerical methods examined herein. For example, a weighted sum of $|\Delta u(y_c)|$, $|\Delta u|_{RSS}$, $|\Delta\phi(0, 1)|$ and $|\Delta\phi(0, \infty)|$ may be computed. Assuming that these quantities are equally important, it is suggested evaluating

$$e(\epsilon) = |\Delta u(y_c)| + |\Delta u|_{RSS} + |\Delta\phi(0,1)| + |\Delta\phi(0,\infty)|. \tag{31}$$

As depicted in Fig. 9, e is maximum in the region $0.1 \lesssim \epsilon \lesssim 1$, except for the B-grid with a no-slip boundary condition. All this is well in agreement with the results presented above.

Table 4
The overall error measure $E(\epsilon_1, \epsilon_2)$ over the segments $0.01 \lesssim \epsilon \lesssim 1$ (non resolved boundary layer), $0.1 \lesssim \epsilon \lesssim 10$ (poorly resolved boundary layer), $1 \lesssim \epsilon \lesssim 100$ (well resolved boundary layer) and $0.01 \lesssim \epsilon \lesssim 100$ (global estimate). The errors are given for the B- and C-grids, with slip and no-slip boundary conditions. The superiority of the solutions obtained with a slip boundary condition is clearly illustrated

	B-grid no-slip	B-grid slip	C-grid no-slip	C-grid slip
$E(0.01, 1)$:	0.75	0.12	0.21	0.12
$E(0.1, 10)$:	0.32	0.11	0.22	0.086
$E(1, 100)$:	0.038	0.033	0.054	0.0062
$E(0.01, 100)$:	0.39	0.076	0.13	0.062

To asses a discrete solution over the range $\epsilon_1 \leq \epsilon \leq \epsilon_2$, it seems quite reasonable to compute an average of $e(\epsilon)$, such as (Table 4)

$$E(\epsilon_1,\epsilon_2) = \frac{\int_{\epsilon_1}^{\epsilon_2} e(\epsilon)\mathrm{d}(\log_{10}\epsilon)}{\log_{10}\epsilon_2 - \log_{10}\epsilon_1}. \quad (32)$$

It is readily seen that $(\log_{10}\epsilon_2 - \log_{10}\epsilon_1)\, E(\epsilon_1, \epsilon_2)$ is the area comprised between the horizontal axis and the relevant curve displayed in Fig. 9. Thus, in a certain sense, definition (32) provides a synthetic view of Fig. 9. Table 4 clearly points to the shortcomings of the B-grid, no-slip solution and puts forward the superiority of the discrete solutions obtained with a slip boundary condition.

5. Conclusions

The coastal boundary layer problem treated here is inspired, in a radiognostic way, from the physical oceanography of the Northern Bering Sea. No stark conclusion, such as Nihoul's, can be drawn. However, the comparison of the discrete along-shore velocity with the exact value is interesting, and sometimes surprising.

First, the thickness of the numerical boundary layer is larger than its exact counterpart.

Second, in most cases, the error affecting the discrete solution is small, whether or not the boundary layer is well resolved by the numerical grid. This is mainly due to the driving force acting over the whole domain, and not just through its boundary — as in Nihoul's example.

Third, the B-grid and C-grid solutions generally exhibit errors of the same order of magnitude, which are maximum when the grid size and the width of the boundary layer are comparable. If the thickness of the boundary layer is much larger, or much smaller, than the space increment, the error is smaller.

Fourth, the slip boundary condition is, in general, the best choice, with a slight advantage to the C-grid.

When the boundary layer is much smaller than the grid size, most of the above conclusions do not apply to the B-grid with a slip boundary condition. In this case, the water flux crossing the grid box adjacent to the coast is in error by a factor of $\approx 1/2$. A fix to this problem has been suggested, but should be tested in a realistic B-grid model — to assess its impact on the flow in the whole computational domain.

Finally, it should be recalled that the problem treated here is an idealized one. Therefore, it is not certain that the results we obtained actually apply to a realistic model. It is however believed that useful guidelines have been provided for further analysis.

Acknowledgements

Professor Nihoul and a anonymous referee provided useful comments on an early version of the manuscript.

References

Bender, C.M. and Orszag, S.A., 1978. Advanced Mathematical Methods for Scientists and Engineers. McGraw-Hill, New York, 593 pp.

Blumberg, A.F. and Mellor, G.L., 1987. A description of a three-dimensional costal ocean circulation model. In: N.S. Heaps (Editor), Three-Dimensional Coastal Ocean Models. Am. Geophys. Union, Washington, D.C., pp. 1–16.

Brasseur, P.P., 1991. A variational inverse method for the reconstruction of general circulation fields in the Northern Bering Sea. J. Geophys. Res., 96: 4891–4907.

Bryan, K., 1969. A numerical method for the study of the circulation of the World Ocean. J. Comput. Phys., 4: 347–376.

Coachman, L.K. and Aagaard, K., 1966. On the water exchange through Bering Strait. Limnol. Oceanogr., 11: 44–59.

Davies, A.M., 1994. Comments on "Do not use a simple model when a complex one will do" — On the complementary nature of observational data, scientific understanding and model complexity: the need for a range of models. J. Mar. Syst., 5(6): 406–408.

Deleersnijder, E., 1994. An analysis of the vertical velocity field computed by a three-dimensional model in the region of the Bering Strait. Tellus, 46A: 134–148.

Deleersnijder, E. and Wolanski, E., 1990. Du rôle de la dispersion horizontale de quantité de mouvement dans les modèles marins tridimensionnels. In: Journées Numériques de Besançon — Courants Océaniques. Publications Mathématiques de Besançon, Besançon, pp. 39–50.

Mellor, G.L. and Blumberg, A.F., 1985. Modeling vertical and horizontal diffusivities with sigma coordinate system. Mon. Weather Rev., 113: 1379–1383.

Nihoul, J.C.J., 1975. Hydrodynamic models. In: J.C.J. Nihoul (Editor), Modelling of Marine Systems. Elsevier, Amsterdam, pp. 41–67.

Nihoul, J.C.J., 1980. Hydrodynamic Models of Shallow Continental Seas. E. Riga Publ., Liège, 198 pp.

Nihoul, J.C.J., 1994. Do not use a simple model when a complex one will do. J. Mar. Syst., 5(6): 401–406.

Overland, J.E. and Roach, A.T., 1987. Northward flow in the Bering and Chukchi Seas. J. Geophys. Res., 92: 7097–7105.

Salomon, J.C., 1994. Comments on "Do not use a simple model when a complex one will do". J. Mar. Syst., 5(6): 408–410.

Spaulding, M., Isaji, T., Mendelsohn, D. and Turner, A.C., 1987. Numerical simulation of wind-driven flow through the Bering Strait. J. Phys. Oceanogr., 17: 1799–1816.

Stigebrandt, A., 1984. The North Pacific: a global scale estuary. J. Phys. Oceanogr., 14:464–470.

Wolfram, S., 1988, Mathematical:A System for Doing Mathematics by Computer. Addison-Wesley, Redwood City, Ca., 749 pp.